JACS
JOURNAL OF THE AMERICAN CHEMICAL SOCIETY
Communication
pubs.acs.org/JACS

Mapping of Molecular Structure of the Nanoscale Surface in Bionanoparticles

Luciana M. Herda, Delyan R. Hristov, Maria Cristina Lo Giudice, Ester Polo,* and Kenneth A. Dawson*

Centre for BioNano Interactions, School of Chemistry, University College Dublin, Belfield, Dublin 4, Ireland

Supporting Information

ABSTRACT: Characterizing the orientation of covalently conjugated proteins on nanoparticles, produced for in vitro and in vivo targeting, though an important feature of such a system, has proved challenging. Although extensive physicochemical characterization of targeting nanoparticles can be addressed in detail, relevant biological characterization of the nanointerface is crucial in order to select suitable nanomaterials for further *in vitro* or *in vivo* experiments. In this work, we adopt a methodology using antibody fragments (Fab) conjugated to gold nanoparticles (immunogold) to map the available epitopes on a transferrin grafted silica particle (SiO_2−PEG_8−Tf) as a proxy methodology to predict nanoparticle biological function, and therefore cellular receptor engagement. Data from the adopted method suggest that, on average, only ∼3.5% of proteins grafted on the SiO_2−PEG_8−Tf nanoparticle surface have a favorable orientation for recognition by the cellular receptor.

Biological recognition and active trafficking in biological systems predominates at the nanoscale. Therefore, in principle, nanotechnology represents an opportunity to formulate novel, nanocarrier-enabled systems with precise, functional properties, determined by the engineering of specific features such as size, shape, chemical composition, surface functionalization and targeting moiety decoration.[1] Although there have been some successes with passive targeting, such as that due to the EPR effect,[2] so far limited progress has been achieved in active targeting of nanoparticle-based therapeutics.[3] The overall reasons for this are still under investigation.[4] However, at least part of the problem may originate in known concerns related to bulk chemical methods to fabricate and functionalize nanoparticles, which are poorly understood. In addition, there are no routinely applied methods to map out molecular detail at the nanoparticle surface (which certainly controls biological interactions).[5] This situation is far removed from that of small molecule drugs, where structure is known in exquisite detail, or that of biological drugs, where the interaction motifs are typically both understood and well characterized structurally.

Here we aim to obtain more precise molecular organizational details, including the availability of receptor recognition motifs of biomolecules presented at the surface of nanoparticles. We use this information as a microscopic basis for design development and ongoing quality characterization of bionanoparticles. By using several kinds of immunoprobe that can identify relevant recognition motifs at the surface of the nanoparticles, we map out structural and organizational aspects of model grafted nanoparticles typical of nanoformulations applied in nanomedicine.[4d,6] In addition, we show it is possible to draw connections between details of nanoparticle design and preparation, and more precise structural characteristics of the system. It is worth noting that therapeutic nanoparticles will typically be structural distributions, with all the potential implications for diversity of biological impact, and it is thus valuable to be able also to characterize this functional diversity.

Transferrin (Tf) protein was grafted onto the poly ethylene glycol (PEG) modified SiO_2 nanoparticle surface using thiol-maleimide chemistry to form SiO_2−PEG_x−Tf (where x denotes different lengths).[4c,d] More specifically, Tf was randomly grafted, through the available primary amine groups, onto the SiO_2 surface modified with a maleimide PEG linker (schematic representation in Figure 1a and Figure S1). Detailed physicochemical characterization of the bionanoparticles and quantification of the protein immobilized on the surface is given in Figure S2. We prepared and characterized immunoprobes (IG and IQD, respectively)[7] consisting of gold nanoparticles (nominal diameter ∼ 4 nm) and quantum dots (QD) (nominal diameter ∼ 4 nm), functionalized with an antigen-binding fragment (Fab) generated from the monoclonal antibody anti-Tf (mAb), which recognizes the epitope aa 142−145, and serves as a proxy for the Tf receptor binding site.[8] Small Fab fragments, generated by using the proteolytic enzyme papain,[9] (Figure S3) were used in order to improve access to the nanoparticle interface. The functionality of Fab was confirmed by dot blot immunoassay (Figure S4).

The biding efficiency of Fab mAb IG and IQD immunolabels (Figures S5−S7) was evaluated by studying their interaction with SiO_2 nanoparticles with a biomolecular corona of Tf protein (adsorbed-on SiO_2@Tf and polystyrene PS@Tf), and similar results to those reported in the literature for polystyrene nanoparticles were obtained(Figure S8).[7a]

We began by studying the interaction between SiO_2−PEG_8−Tf particles and Fab mAb IG. To ensure that all sites available to the IG labels were accessed, we titrated the nanoparticles to the saturation point by using differential centrifugal sedimentation (DCS) (Figure 1b). When saturation was achieved (Figure 1c), samples were analyzed by transmission electron microscopy (TEM) (Figure 1d, see control in Figure S9). TEM imaging of sufficient quantities of the SiO_2−PEG_8−Tf particle-IG complexes allowed us to construct the distribution of

Received: November 29, 2016
Published: December 22, 2016

DOI: 10.1021/jacs.6b12297
J. Am. Chem. Soc. 2017, 139, 111−114

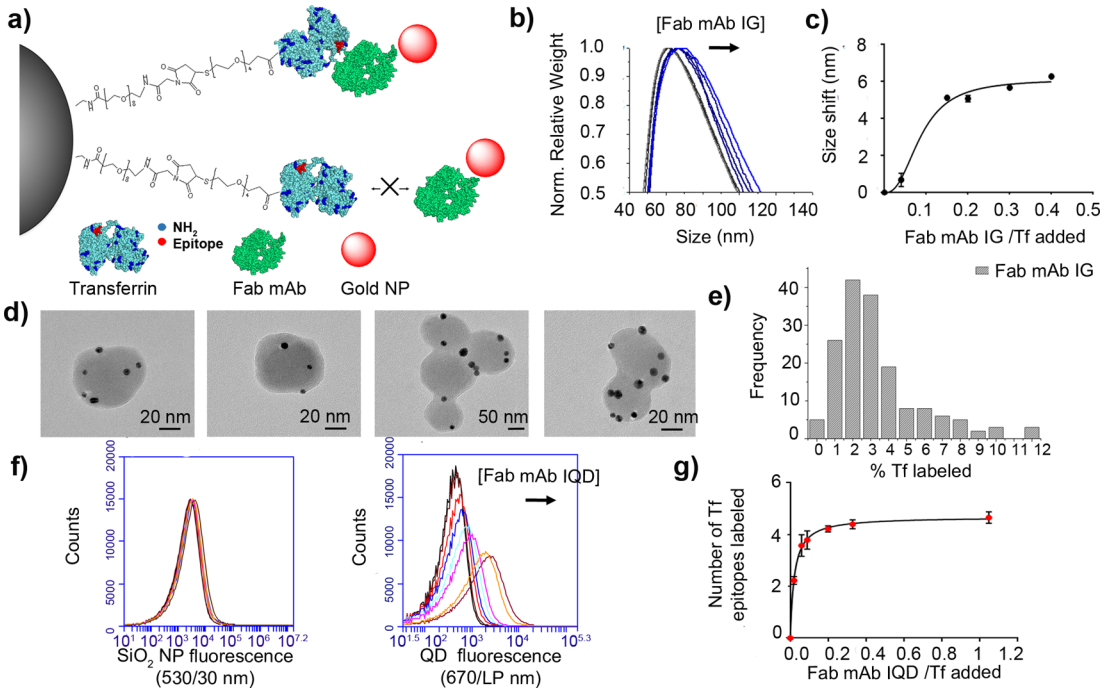

Figure 1. Epitope mapping of SiO_2−PEG_8−Tf nanoparticle surface. (a) Schematic representation of the mechanism of interaction between Tf grafted silica nanoparticles and immunolabels (Fab mAb IG). (b) DCS measurements of Fab mAb IG titrated to SiO_2−PEG_8−Tf particles. (c) Fitting analysis of the shift in the apparent size of the bionanoparticle, considered as indicative of the titration saturation point, versus the IG added per SiO_2−PEG_8−Tf . (d) Representative TEM micrographs of SiO_2−PEG_8−Tf particles labeled with Fab mAb IG at saturation. (e) Histogram representing the total number of IG labels per SiO_2−PEG_8−Tf particle counted by TEM. (f) Flow cytometry histograms represent the mean fluorescence of each sample of SiO_2−PEG_8−Tf particles (left) and SiO_2−PEG_8−Tf particles labeled with increasing concentration of Fab mAb QDs (right). (g) Number of IQDs labels per silica nanoparticle as obtained from fluorescence spectroscopy.

available epitopes on the nanoparticle surface (Figure 1e). The convergence of the distributions in TEM was checked by the progressive addition of measured particles to the analysis (Figure S10). Using DCS, we determined the saturation point of the Fab mAb IG SiO_2−PEG_8−Tf interaction at 0.15−0.2 IG labels added per Tf whereas the Tf labeled fraction observed by TEM was only between 3 and 4% of the total grafted protein (Figure 1e). Our results by TEM immunolabeling also suggest a high relative epitope variability in the particle-to-particle analysis. This striking result indicating the presence of a small accessible Tf fraction was confirmed using Fab mAb IQD as reporter binders following the procedure described in[7b] (Figure 1f). SiO_2−PEG_8−Tf nanoparticles were incubated with Fab mAb IQD (synthesis and functionalization in Figures S7) and the fluorescent signal was measured and compared to a calibration curve (Figure S7d). 4% of the total protein grafted onto SiO_2−PEG_8−Tf particles was detected by IQD labels (Figure 1g). Using these techniques together allows for a comprehensive estimation of the accessible fraction of Tf epitopes on the particle surface. Moreover, TEM mapping methodology allows us to estimate the relevant biological functionality of the targeting NP and, significantly, the particle-to-particle and batch-to-batch variability.

The low percentage of labeled Tf fraction on the bionanoparticles could be explained by the denaturation of the protein after grafting, by the protein chemical modification (PEGylation), Tf molecular crowding on the particle surface, unfavorable Tf grafting orientation, or Tf partial occlusion by penetrating in PEG layer.[10] The first and second concerns were studied by mapping the surface of Tf adsorbed-on particles (SiO_2@Tf) where the protein was previously modified to various degrees of PEGylation. TEM measurements of modified SiO_2@Tf particles showed no observable impact of the accessible epitope fraction by protein PEGylation (Figure S11). The molecular crowding effect was investigated by grafting different Tf densities on SiO_2−PEG_8−Tf particles. An increase in the Tf fraction labeled by IG, from 1 to ∼4%, was observed by increasing the Tf density grafted on the particle surface (Figure 2a). These results suggest that the grafting methodology has the greatest impact on epitope accessibility (Figure S12 for available primary amines on Tf). Improving the design of surface ligand architecture could potentially address some of the challenges in the accessibility and functionality of bionanoparticles.

Through the use of linkers of various lengths and, in a more advanced scenario, a bifunctional layer, we attempted to elucidate further the relationship between ligand architecture and epitope accessibility (Figure 2b,c). In the latter case a long, functional PEG_8 or PEG_{24} ligand enables protein grafting while a short, inert PEG_4 ligand is used to improve nanoparticle stability and provide "stealth" properties by inhibiting protein adsorption.[11] We hypothesize that, as ligand mobility increases, the probability of successful antibody−protein recognition is increased. We observed an increase in Tf labeling on mixed ligand SiO_2−PEG_x−Tf particles when compared to one PEG size architecture with comparable protein coverage, by TEM mapping (Figure 2b and S13). Once it was confirmed that the long functional (PEG_{24}) ligand effectively improves epitope accessibility, we studied the relationship between the degrees of freedom of the long PEG linker and the accessible Tf fraction by TEM. A scenario with a more mobile architecture (low density of long PEG chains by increasing molar ratio

DOI: 10.1021/jacs.6b12297
J. Am. Chem. Soc. 2017, 139, 111−114

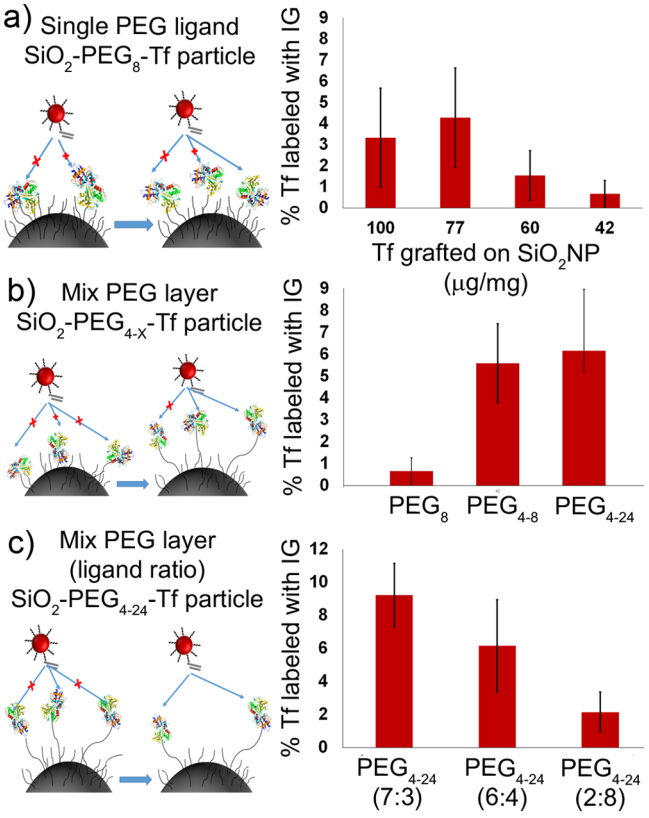

Figure 2. Fraction of transferrin grafted onto silica nanoparticles labeled with Fab mAb IG and measured by TEM. (a) Tf grafted silica nanoparticles with one, single length PEG (PEG_8) and different surface densities of Tf immobilized on the nanoparticle. (b) Comparison of Tf grafted silica nanoparticles designed with different PEG architectures, consisting of two mixed PEG length ligands: one short, inert PEG linker (PEG_4) and one long, functional PEG linker (PEG_8 and PEG_{24}). (c) Comparison of Tf grafted silica nanoparticles designed with a mixed PEG layer of different ratio of PEG_4 and PEG_{24}.

PEG_4:PEG_{24}) allows for a higher number of proteins to be recognized (Figure 2c, and S13). A larger study needs to be conducted to elucidate fully the relationship between PEG lengths, functional ligand mobility and the labeled well oriented protein fraction. Our results (Table 1) suggest that such a relationship exists and it is likely that further design improvements on ligand functionality could lead optimized epitope accessibility.

To summarize, we have demonstrated the potential for immunolabeling techniques to be used in the design phase of protein grafted nanoparticles and promote their ongoing quality control, both key issues requiring immediate advances. Immunolabeling using antibody fragments that actively bind to the antigen molecule (for example, locations that proxy for the receptor interaction site) provides relevant biological characterization for the design of targeted nanoparticles.

Though the interactions described here are not fully representative of protein−receptor interactions, they have provided a better understanding of the structural details of a protein grafted in a particle-by-particle manner that is linked more directly to what "cells see".[12] Together, our results suggest that the epitope accessibility of SiO_2−PEG_8−Tf particles is low (approximately 4%). Although PEG length control and ligand layer architecture can enhance this somewhat (∼10%), the overall impression is that standard methods currently in use to graft targeting ligands may lead to quite poor (and heterogeneous) outcomes. There can be little doubt that some of these limitations are due to the random coupling procedures currently in use, which could be readily improved upon by developments in chemical ligation approaches. Though, we cannot be sure that they are a major cause of the difficulties currently reported in targeting studies we do feel certain that they are at least partly involved in those issues. It is clear that improvements in approach are required, and possible, and should be made before further conclusions are drawn about the efficacy of ligated nanomedicines.

Table 1. Tf Grafted SiO_2 Particles Prepared with Different Ligand Architectures

	μg Tf/mg NP	N° Tf/NP	Average (%)	S.D.
PEG_8	100	108	3.3	2.3
PEG_8	77	83	4.3	2.3
PEG_8	60	65	1.5	1.2
PEG_8	42	45	0.7	0.6
PEG_{4-8} (7 to 3)	48	52	5.6	1.8
PEG_{4-24} (9 to 1)	23	25	5.5	1.3
PEG_{4-24} (7 to 3)	25	27	9.2	1.9
PEG_{4-24} (6 to 4)	43	46	6.2	2.8
PEG_{4-24} (2 to 8)	49	53	2.1	1.2

■ ASSOCIATED CONTENT

Supporting Information

The Supporting Information is available free of charge on the ACS Publications website at DOI: 10.1021/jacs.6b12297.

Experimental details and Figures S1−S13 (PDF)

■ AUTHOR INFORMATION

Corresponding Authors

*Kenneth.a.dawson@cbni.ucd.ie

*Ester.polotobajas@cbni.ucd.ie

ORCID

Ester Polo: 0000-0001-8870-5280

Author Contributions

L.M.H. and D.R.H. contributed equally.

Funding

EU Marie Curie PATHCHOOSER project (PITN-GA-2013-608373). EU FP7 FutureNanoNeeds project (604602). Science Foundation Ireland (SFI, 12/IA/1422).

Notes

The authors declare no competing financial interest.

■ ACKNOWLEDGMENTS

L.M.H. acknowledges the EU Marie Curie PATHCHOOSER project (PITN-GA-2013-608373). D.R.H. acknowledges EU FP7 FutureNanoNeeds project (Agreement No. 604602). E.P., M.C.L.G. and K.A.D. acknowledge the Science Foundation Ireland (SFI, 12/IA/1422). UCD Conway Imaging and Flow Cytometry Cores are also acknowledged.

■ REFERENCES

(1) (a) Albanese, A.; Tang, P. S.; Chan, W. C. W. *Annu. Rev. Biomed. Eng.* **2012**, *14*, 1. (b) Ferrari, M. *Nat. Nanotechnol.* **2008**, *3*, 131. (c) Parak, W. J. *Science* **2016**, *351*, 814. (d) Shi, J.; Kantoff, P. W.; Wooster, R.; Farokhzad, O. C. *Nat. Rev. Cancer* **2016**, *17*, 20. (e) Parodi, A.; Quattrocchi, N.; van de Ven, A. L.; Chiappini, C.;

DOI: 10.1021/jacs.6b12297
J. Am. Chem. Soc. 2017, 139, 111−114

Evangelopoulos, M.; Martinez, J. O.; Brown, B. S.; Khaled, S. Z.; Yazdi, I. K.; Enzo, M. V.; Isenhart, L.; Ferrari, M.; Tasciotti, E. *Nat. Nanotechnol.* **2013**, *8*, 61.
(2) (a) Acharya, S.; Sahoo, S. K. *Adv. Drug Delivery Rev.* **2011**, *63*, 170. (b) Allen, T. M.; Cullis, P. R. *Adv. Drug Delivery Rev.* **2013**, *65*, 36. (c) Dhar, S.; Gu, F. X.; Langer, R.; Farokhzad, O. C.; Lippard, S. *Proc. Natl. Acad. Sci. U. S. A.* **2008**, *105*, 17356.
(3) Min, Y.; Caster, J. M.; Eblan, M. J.; Wang, A. Z. *Chem. Rev.* **2015**, *115*, 11147.
(4) (a) Wilhelm, S.; Tavares, A. J.; Dai, Q.; Ohta, S.; Audet, J.; Dvorak, H. F.; Chan, W. C. W. *Nat. Rev. Mater.* **2016**, *1*, 16014. (b) Schöttler, S.; Becker, G.; Winzen, S.; Steinbach, T.; Mohr, K.; Landfester, K.; Mailänder, V.; Wurm, F. R. *Nat. Nanotechnol.* **2016**, *11*, 372. (c) Salvati, A.; Pitek, A. S.; Monopoli, M. P.; Prapainop, K.; Bombelli, F. B.; Hristov, D. R.; Kelly, P. M.; Aberg, C.; Mahon, E.; Dawson, K. A. *Nat. Nanotechnol.* **2013**, *8*, 137. (d) Hristov, D. R.; Rocks, L.; Kelly, P. M.; Thomas, S. S.; Pitek, A. S.; Verderio, P.; Mahon, E.; Dawson, K. A. *Sci. Rep.* **2015**, *5*, 17040.
(5) (a) Mortimer, G. M.; Butcher, N. J.; Musumeci, A. W.; Deng, Z. J.; Martin, D. J.; Minchin, R. F. *ACS Nano* **2014**, *8*, 3357. (b) Fleischer, C. C.; Payne, C. K. *J. Phys. Chem. B* **2014**, *118*, 14017. (c) Treuel, L.; Brandholt, S.; Maffre, P.; Wiegele, S.; Shang, L.; Nienhaus, G. U. *ACS Nano* **2014**, *8*, 503.
(6) Sapsford, K. E.; Algar, W. R.; Berti, L.; Gemmill, K. B.; Casey, B. J.; Oh, E.; Stewart, M. H.; Medintz, I. L. *Chem. Rev.* **2013**, *113*, 1904.
(7) (a) Kelly, P. M.; Åberg, C.; Polo, E.; O'Connell, A.; Cookman, J.; Fallon, J.; Krpetić, Ž.; Dawson, K. A. *Nat. Nanotechnol.* **2015**, *10*, 472. (b) Lo Giudice, M. C.; Herda, L. M.; Polo, E.; Dawson, K. A. *Nat. Commun.* **2016**, *7*, 13475.
(8) Cheng, Y.; Zak, O.; Aisen, P.; Harrison, S. C.; Walz, T. *Cell* **2004**, *116*, 565.
(9) Rawlings, N. D.; Barrett, A. J. *Proteolytic Enzymes: Serine and Cysteine peptidases*; Methods in Enzymology Series; Elsevier, 1994.
(10) Pelaz, B.; Del Pino, P.; Maffre, P.; Hartmann, R.; Gallego, M.; Rivera-Fernandez, S.; De la Fuente, J. M.; Nienhaus, G. U.; Parak, W. J. *ACS Nano* **2015**, *9*, 6996.
(11) (a) Dai, Q.; Walkey, C.; Chan, W. C. W. *Angew. Chem., Int. Ed.* **2014**, *53*, 5093. (b) Ishii, T.; Miyata, K.; Anraku, Y.; Naito, M.; Yi, Y.; Jinbo; Takae, S.; Fukusato, Y.; Hori, M.; Osada, K.; Kataoka, K. *Chem. Commun.* **2016**, *52*, 1517. (c) Lo Giudice, M. C.; Meder, F.; Polo, E.; Thomas, S. S.; Alnahdi, K.; Lara, S.; Dawson, K. A. *Nanoscale* **2016**, *8*, 16969.
(12) (a) Lynch, I.; Dawson, K. A.; Linse, S. *Sci. STKE* **2006**, *327*, 14. (b) Walczyk, D.; Bombelli, F. B.; Monopoli, M. P.; Lynch, I.; Dawson, K. A. *J. Am. Chem. Soc.* **2010**, *132*, 5761.

DOI: 10.1021/jacs.6b12297
J. Am. Chem. Soc. 2017, 139, 111−114